## **Huimin Zhou**

Department of Systems Science and Industrial Engineering, Binghamton University, Binghamton, NY 13902

## **Yingchun Jiang**

Department of Mechanical Engineering, Binghamton University, Binghamton, NY 13902

## Changhong Ke

Department of Mechanical Engineering, Binghamton University, Binghamton, NY 13902; Materials Science and Engineering Program, Binghamton University, Binghamton, NY 13902

# Jia Deng<sup>1</sup>

Department of Systems Science and Industrial Engineering, Binghamton University, Binghamton, NY 13902 e-mail: jiadeng@binghamton.edu

# Electric-Field and Mechanical Vibration-Assisted Atomic Force Microscope-Based Nanopatterning

Atomic force microscope (AFM)-based nanolithography is a cost-effective nanopatterning technique that can fabricate nanostructures with arbitrary shapes. However, existing AFM-based nanopatterning approaches have limitations in the patterning resolution and efficiency. Minimum feature size and machining performance in the mechanical forceinduced nanofabrication process are limited by the radius and sharpness of the AFM tip. Electric-field-assisted atomic force microscope (E-AFM) nanolithography can fabricate nanopatterns with features smaller than the tip radius, but it is very challenging to find the appropriate input parameter window. The tip bias range in E-AFM process is typically very small and varies for each AFM tip due to the variations in tip geometry, tip end diameter, and tip conductive coating thickness. This paper demonstrates a novel electric-field and mechanical vibration-assisted AFM-based nanofabrication approach, which enables high-resolution (sub-10 nm toward sub-5 nm) and high-efficiency nanopatterning processes. The integration of in-plane vibration with the electric field increases the patterning speed, broadens the selectable ranges of applied voltages, and reduces the minimum tip bias required for nanopatterning as compared with E-AFM process, which significantly increases the versatility and capability of AFM-based nanopatterning and effectively avoids the tip damage. [DOI: 10.1115/1.4056731]

Keywords: atomic force microscope, electric field, vibration, nanopatterning, nanolithography, nanofabrication

## Introduction

In line with current advanced nanotechnology, the study of nanostructures has attracted increasing interest in various research fields that range from optoelectronics and nano-electronics to biomedicine and energy [1–4]. To date, there are several technologies that are widely used in fabricating nanostructures. Photolithography, soft lithography, and nano-imprint techniques, which require photomasks or molds, enable nanomanufacturing with high throughput [5-7]. Meanwhile, maskless approaches, including electron-beam lithography, focused ion beam lithography, twophoton lithography, and atomic force microscope (AFM)-based nanofabrication, can build high-resolution masks and molds for parallel nanopatterning techniques [2,8–10]. Electron-beam lithography generates patterns by emitting electrons on photoresists. Similarly, focused ion beam lithography uses a focused beam of ions to bombard the sample and modify the surface structure. Both the electron-beam lithography and focused ion beam lithography are capable of creating fine features, but the processes are costly and have low fabrication yields [11]. In contrast to the techniques that use electrons, ions, or photons, the AFM-based nanopatterning technique is a single-step process that is capable of generating high-resolution nanopatterns using ultrasharp AFM probes without subsequent development steps [12]. It has shown great potential to fabricate high-resolution features with unprecedented technical capabilities [13,14].

Atomic force microscope-based nanopatterning exhibits many advantages. It is cost-effective for implementation and

maintenance, is capable of operating in the ambient environment with fast patterning speed, and is suitable for a variety of materials that include polymers, silicon, metals, and 2D materials [15–21]. It can also obtain sub-10 nm nanofeatures through localized physical and chemical reactions [22]. Due to the severe tip wear caused by large contact force in the direct machining of hard materials, many studies investigated the AFM-based lithography on polymer thin films that are spin-coated on hard surfaces, such as silicon or silicon oxide [23,24]. After lithography, nanopatterns generated on polymer films can be further etched onto substrate materials, which reduce tip wear and therefore extend tip's lifetime [2]. This technique has been widely applied because soft polymers are widely used as masks or resists in electronic device fabrication [25].

In AFM tip-based nanolithography, nanostructures are fabricated by means of adding an external stimulus to the tip, which results in physical or chemical reactions localized to the tipsurface junction when the AFM tip is positioned at or close to the substrate [26]. The tip-sample interactions include mechanical, thermal, chemical, and electric fashions [27]. In the mechanical interactions, substrate materials are removed by the effect of mechanical force, which is applied in techniques such as dynamic plowing [28], direct machining [29,30], and vibration-assisted lithography [31]. The thermal effect used in AFM-based thermal writing locally modifies substrate material properties through a heated AFM probe by a resistive heater integrated on the cantilever [32,33]. Generally, local modifications of material properties include material removal, conversion through chemical reactions activated by heat, and material addition through melting or deposition [34]. Thermal energy can also be applied through a sample heating method instead of probe heating to soften polymer samples under elevated temperatures, which facilitates the machining process [35]. Electric-field-assisted AFM lithography, or the socalled bias-assisted AFM lithography process, involves highly

<sup>&</sup>lt;sup>1</sup>Corresponding author.

Contributed by the Manufacturing Engineering Division of ASME for publication in the JOURNAL OF MICRO- AND NANO-MANUFACTURING. Manuscript received September 30, 2022; final manuscript received January 9, 2023; published online February 1, 2023. Assoc. Editor: TieJun Zhang.

confined joule heating, local oxidation, field emission, and electrostatic interactions [27,36–38].

Two typical electric-field-assisted AFM techniques are AFMassisted electrostatic lithography (AFMEN) and field-emission scanning probe lithography [37,39]. AFM-assisted electrostatic lithography generates nanopatterns by utilizing the current flow between AFM tip and conductive substrate, while the other selectively crosslinks or scissors polymer resist through Fowler-Nordheim (FN) field emission of low energy electrons. However, a distance between tip-polymer surface leads to the formation of large features. Zhou et al. [40] proposed and demonstrated an electric-field-assisted contact mode AFM-based method using soft probes, which is capable of fabricating high-resolution nanopatterns with feature width down to  $\sim$ 16 nm [40]. But it remains difficult to identify the correct tip bias range for nanopatterning. If the applied tip bias is too small, it cannot fabricate any nanopatterns. Conversely, if the applied tip bias is too large, it can lead to tip damage.

In vibration-assisted AFM-based lithography, the application of in-plane and out-of-plane vibration on the substrate helps increase the patterning speed, enables tunable nanopattern feature size, and enhances the nanomachining performance [20]. However, the minimum feature width fabricated by vibration-assisted AFM-based lithography is limited by the tip size, and the mechanical force-induced processes usually generate a significant amount of debris along the side of patterns.

Each single energy-induced AFM-based lithography process has its limitations. It is advantageous to involve multiple energy forms to improve the nanopatterning performances. Existing combinations include coupling AFM lithography, which applies both force load and bias voltage simultaneously in the AFM lithography process. It is proved that the coupling effect helps to fabricate patterns with larger depth and lower surface roughness as compared with each individual technique alone (i.e., either mechanical force-induced or electric-field-induced AFM lithography [41]). Another approach is a thermal and vibration-assisted AFM based

nanolithography proposed by Zhou et al. [35], which also enhanced the nanomachining performances through the integration of heating and vibration energy.

This article innovates an electric-field and mechanical vibration-assisted AFM-based (E-V AFM) nanopatterning approach using soft conductive probes. Through the integration of electric field and mechanical vibration, this approach greatly increases the nanopatterning performances, which include high resolution (sub-10 nm feature width that is close to 5 nm), less debris as compared with mechanical force induced nanolithography, and higher patterning speed as compared with only either vibration or electric-field-assisted processes. This new process increases the patterning efficiency, broadens the selectable ranges of applied voltages, and reduces the minimum tip bias required for nanopatterning. In addition, it provides expanded feature size range and a better control of the fabricated nanofeature dimensions.

### **Experimental Setup and Mechanisms**

The electric-field and mechanical vibration-assisted AFM nanolithography experiments were performed based on a commercial AFM (XE7, Park Systems Corporation) with a high-voltage toolkit, which includes a voltage amplifier with an amplification ratio of 17.5. Note that the actual values of tip bias mentioned in this paper were calculated as the input values multiply by the 17.5 gain. An in-house fabricated nanolithography stage was used to integrate the electric-field and mechanical vibration for nanopatterning processes. A schematic of the experimental setup is shown in Fig. 1(a). Two piezo-actuators (SA050510, Piezo-Drive) were attached on the aluminum nanolithography stage to generate vibrations in both x and y directions. The entire setup was placed inside an acoustic enclosure, which helps isolate external sound and vibration to better control the machining performances. The sample is prepared by first electron-beam evaporation of an Au layer (100 nm thickness) on a silicon substrate, followed by

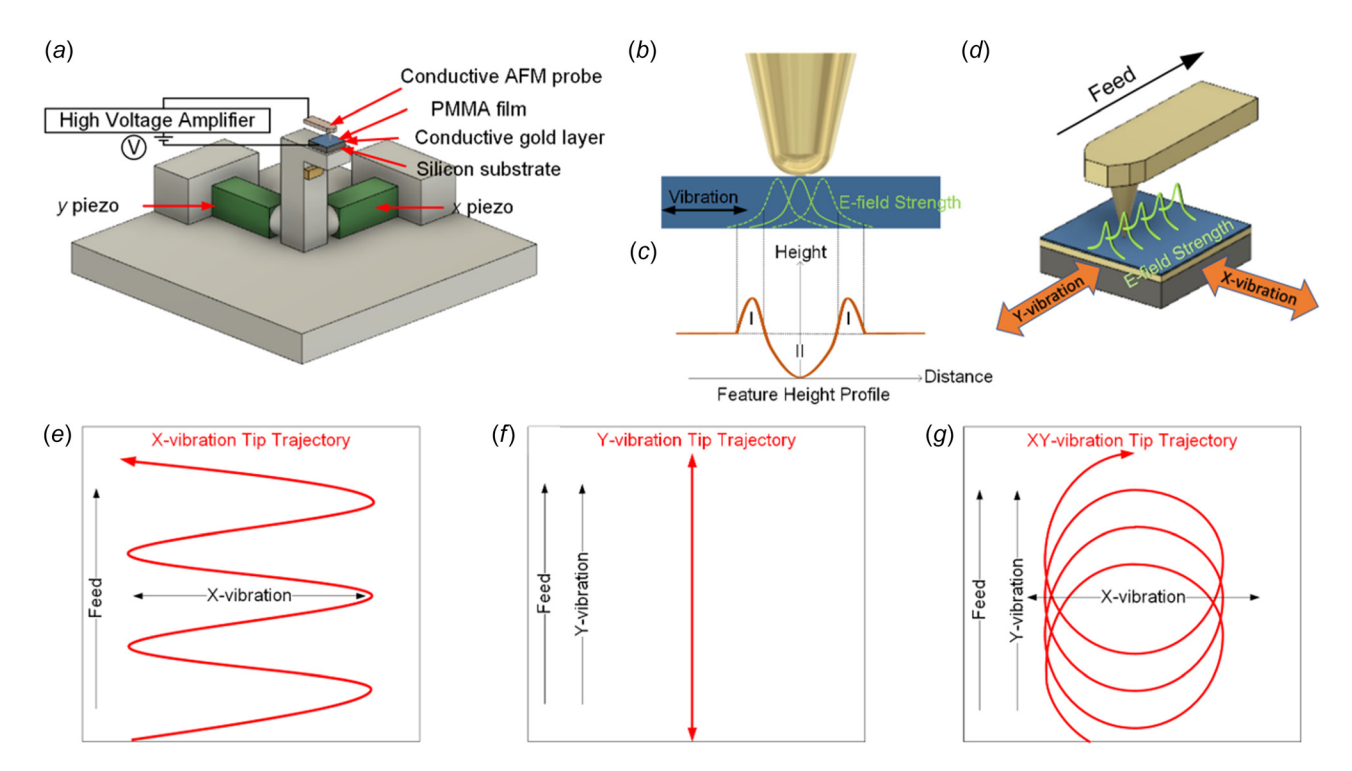


Fig. 1 A Schematic illustration of the experimental setup and the mechanism of the E-V AFM nanolithography. (a) A schematic view of the E-V AFM setup. (b) E-field strength distribution in the polymer layer underneath the AFM tip. (c) Height profile of the fabricated nanofeatures corresponding to the e-field strength in (b). (d) A schematic illustration of the electric-field strength distribution in x-z plane as the tip moves in the nanolithography process. Schematic views of the AFM tip trajectories in E-V AFM-based nanopatterning with (e) x-vibration, (f) y-vibration, and (g) xy-vibration.

Table 1 Specifications of the AFM probes

AFM probe type	Nominal tip radius (nm)	Tip material	Nominal spring constant (N/m)	Function
CSG10/TiN	35	Si + TiN coating	0.11	Lithography and scanning Scanning
ContAl-G	10	Si	0.2	

spin-coating a 50 nm polymethyl methacrylate (PMMA) layer. After that, the sample was baked at 180 °C for 90 s. A conductive AFM probe (CSG10/TiN) with conductive TiN coatings on both the tip side and the back side was used in contact mode lithography, in which small constant contact forces (~0.1 nN) were applied between the AFM tip and the sample. Table 1 shows the specifications of the AFM probes that were used in lithography and in scanning processes.

A previous study of Zhou et al. [40] demonstrated that the contact mode electric-field-assisted AFM (E-AFM)-based process can fabricate high-resolution nanopatterns. In the process, polymer films are selectively removed by the localized electric breakdown created by the bias between AFM tip and conductive layer of the sample substrate. This study developed an ANSYS simulation model that generates the electric-field (e-field) strength distribution in the polymer film right underneath the AFM tip in the E-AFM

nanolithography process [40]. The e-field strength distributes like a bell-shaped curve that has its maximum value in the center, and gradually decreases along the sides, as illustrated in Fig. 1(b). The depths of fabricated nanofeatures correspond to the e-field strength, with a front view showing in Fig. 1(c). In the center part where the e-field strength is extremely large, joule heating generated by the flow of electrons lead to the local sublimation of polymer underneath, which is shown as area II in Fig. 1(c). In the area where the joule heating is not large enough for polymer sublimation, the temperature can still be high enough to soften the polymer. The softened polymer was then pressed and pushed aside by the AFM tip with the in-plane vibration, which is described as the extruded feature (area I) in Fig. 1(c). When the same tip bias is applied, the same e-field strength distribution exists at every point of the tip trajectory when the tip moves along the feeding direction, as is shown in Fig. 1(d). Note that this image only shows the

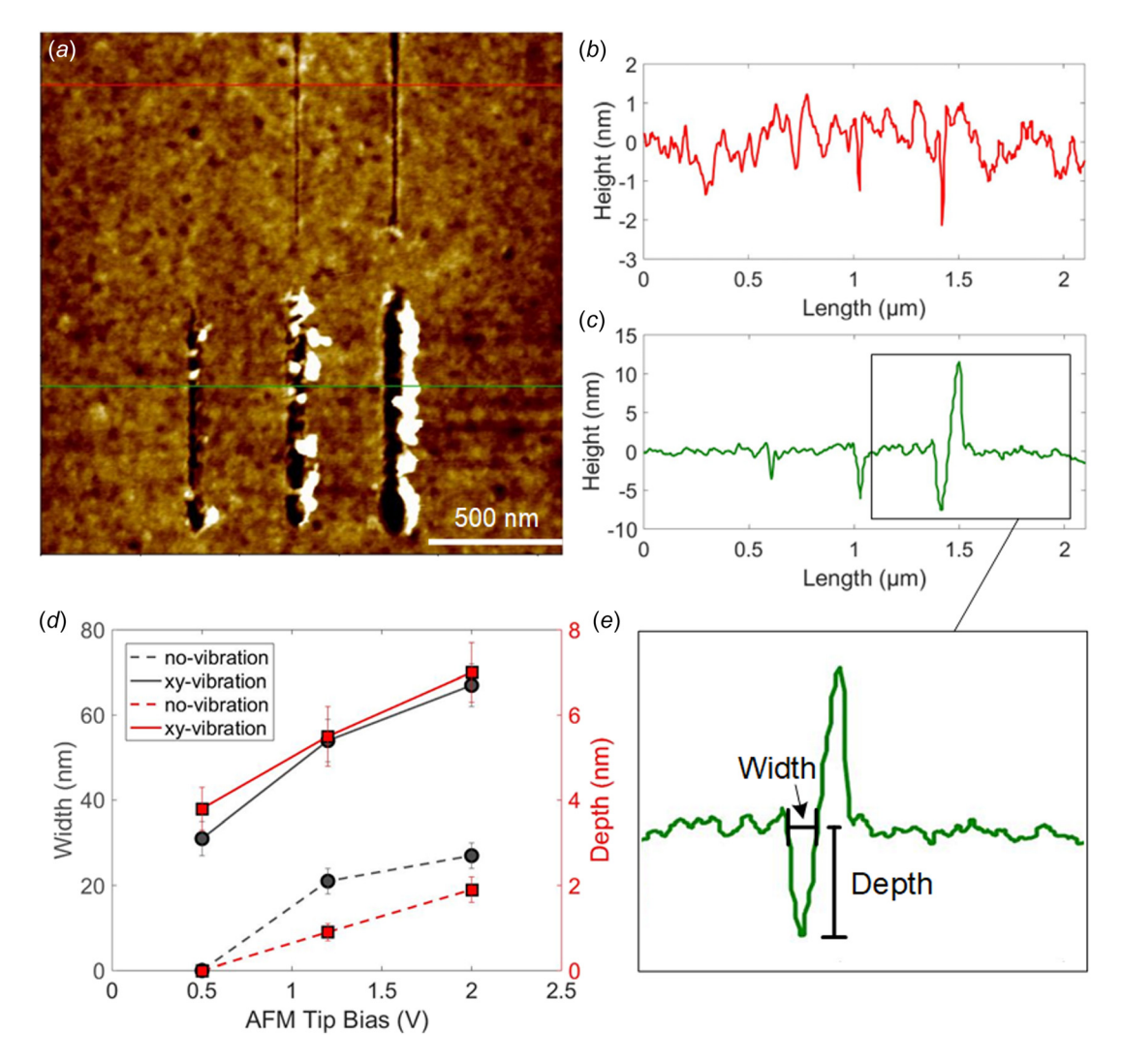


Fig. 2 E-V AFM lithography results with no-vibration (upper three lines) and xy-vibration (lower three lines, vibration amplitude = 0.6 VPP) under different tip biases (0.5, 1.2, 2 V from left to right, respectively). (a) Topography image of the nanopatterns. (b) and (c) Height profiles of nanotrenches without and with vibration. (d) Widths and depths of trenches fabricated with and without vibration under different tip biases. (e) An illustration of trench width and depth measurement.

e-field strength distribution in x–z plane, but the same distribution applies in all the planes along the z axis. Therefore, the joule heating at a certain point of the tip trajectory is an accumulation of energy as the tip passes through the nearby region.

The integration of in-plane mechanical vibration in the E-V AFM nanolithography process not only increase the patterning speed and machining efficiency, but also adds more flexibility in the dimensions of fabricated nanofeatures, which is described as follows.

Figures 1(e)-1(g) include schematic views of the AFM tip trajectory with different vibration settings, which is beneficial for the understanding of the fabricated feature dimensions. Figure 1(e) illustrates the tip trajectory when only the *x*-vibration is integrated, in which the direction of mechanical vibration is perpendicular to the tip feeding direction. The tip trajectory shows as a zigzag shape with the dimensions determined by tip feed rate and

x-vibration frequency and amplitude. If only y-vibration is added, and the tip feeding direction is parallel to the direction of mechanical vibration, the tip goes back and forth along the same line when it moves toward the feeding direction, as is shown in Fig. 1(f). When both x and y vibrations are added which leads to a circular vibration of the sample [42], the tip has a circular trajectory that moves toward the feeding direction, as is shown in Fig. 1(g). As is indicated above, the nanofeatures are fabricated by localized electric breakdown and polymer sublimation. Comparing to the tip trajectory of E-V AFM with x-vibration, tip trajectory of E-V AFM with y-vibration is within a single line, which represents intensive energy accumulation in a smaller area. Due to the difference in energy accumulation, it is likely that the integration of y-vibration in the E-V AFM process helps to create narrower but deeper trenches comparing to the E-V AFM setup with x-vibration. In the meantime, the edge of trenches fabricated by

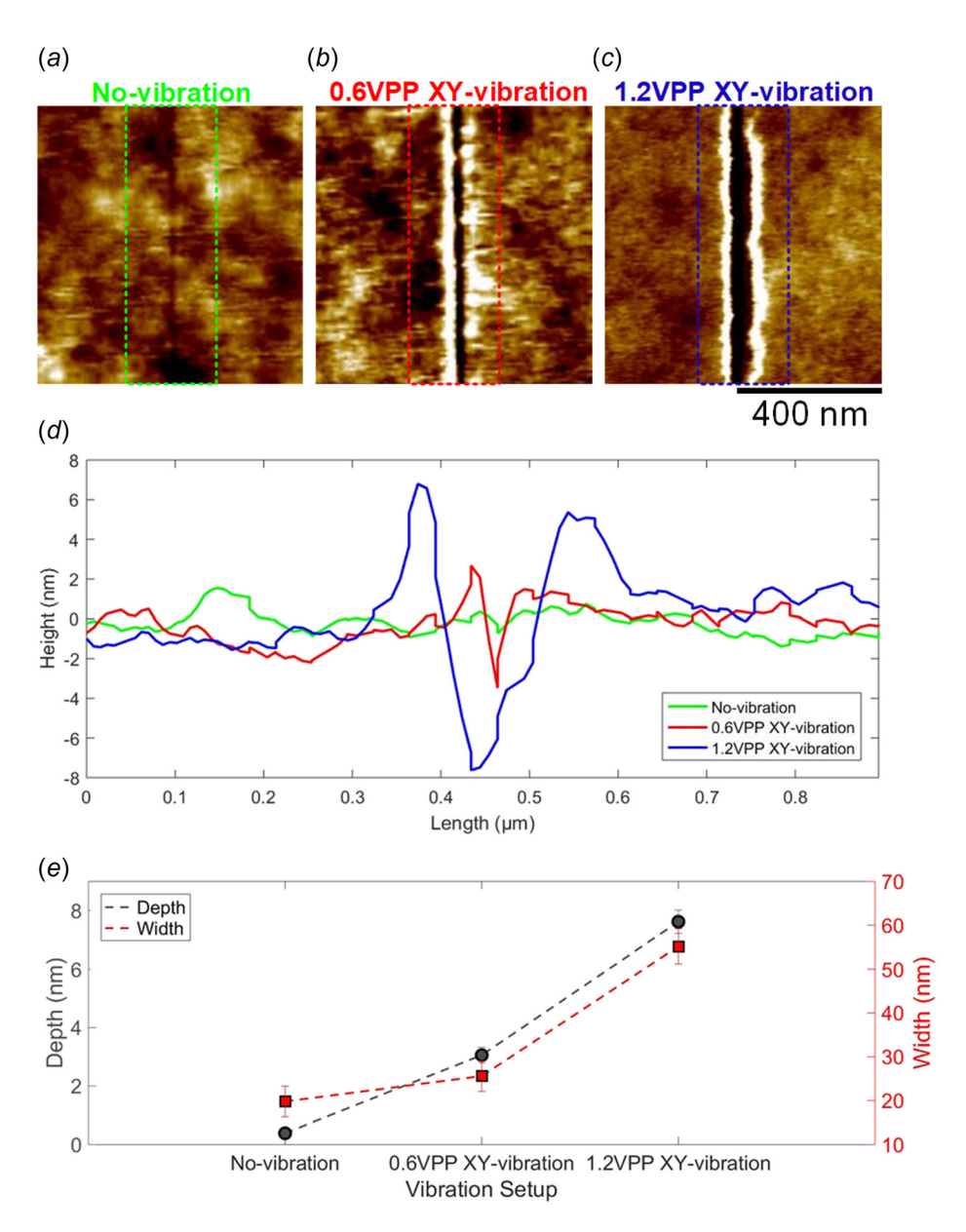


Fig. 3 E-V AFM lithography results with different xy-vibration amplitudes (vibration amplitude = 0, 0.6, and 1.2 VPP) comparison, with the same speed (0.5  $\mu$ m/s) and tip bias (2.9 V) applied. (a)–(c) Topography images. (d) Height profiles of topography images. (e) Width and depth comparison of the trenches fabricated with different xy-vibration amplitudes.

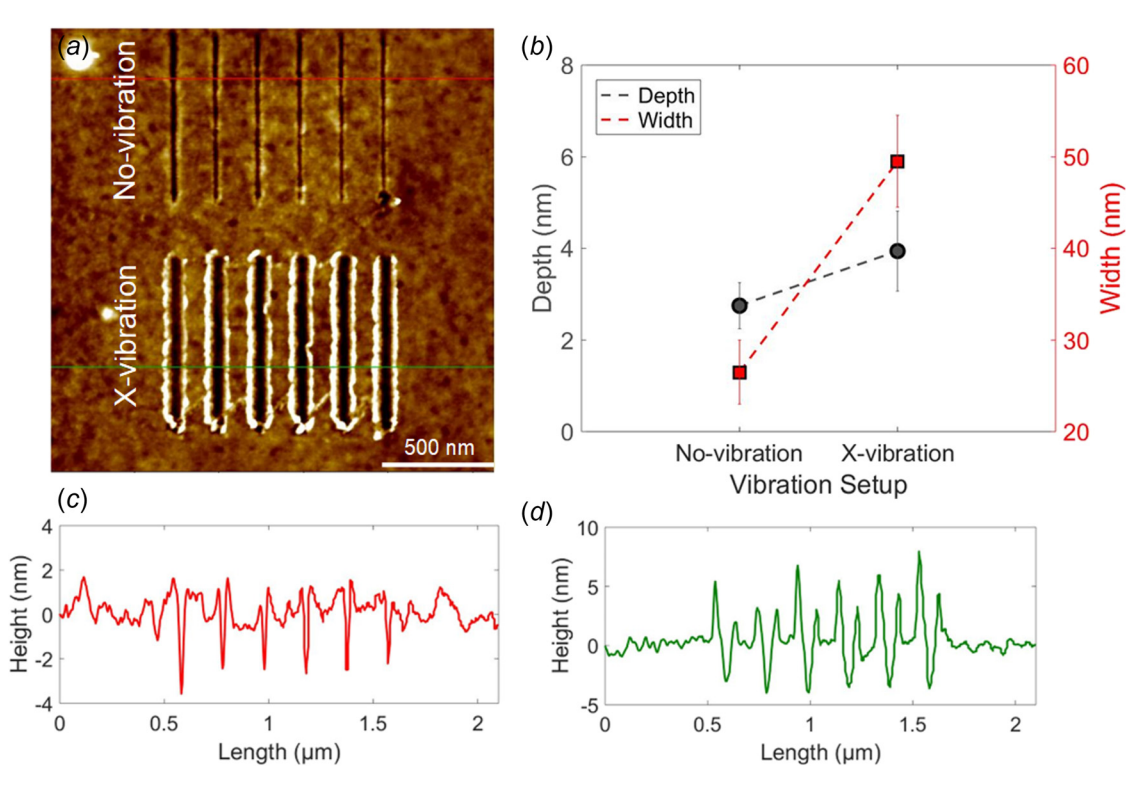


Fig. 4 E-V AFM lithography results with no-vibration and *x*-vibration (vibration amplitude = 0.6 VPP) comparison, with the same tip bias (2.1 V) applied. (a) Topography image of the nanopatterns. (b) Widths and depths of trenches fabricated with and without *x*-vibration. (c) and (d) Height profile of nanotrenches with no-vibration and *x*-vibration.

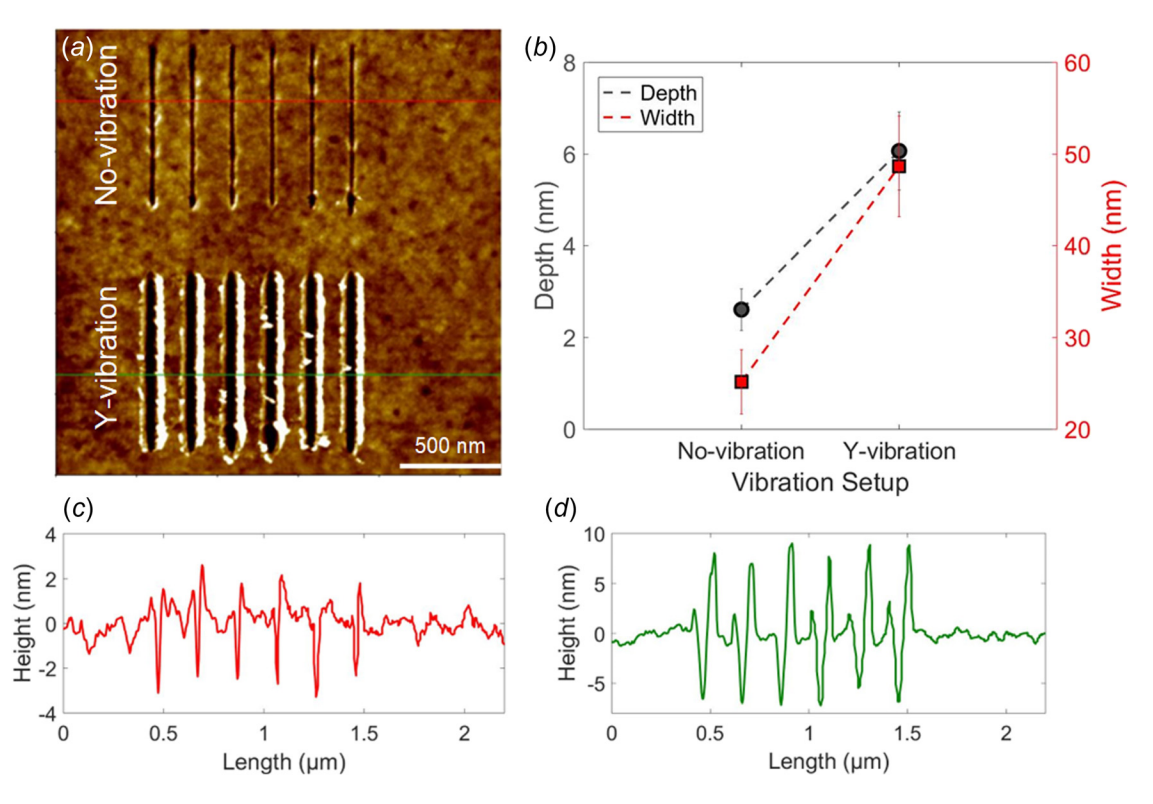


Fig. 5 E-V AFM lithography results with no-vibration and *y*-vibration (vibration amplitude = 0.6 VPP) comparison, with the same tip bias (2.1 V) applied. (a) Topography image of the nanopatterns. (b) Widths and depths of trenches fabricated with and without *y*-vibration. (c) and (d) Height profiles of nanotrenches with no-vibration and *y*-vibration.

*xy*-vibration integrated E-V AFM could be more uniform based on the performance of *xy*-vibration in mechanical force induced AFM nanolithography experiments.

## **Experimental Results and Discussions**

In this study, multiple nanopatterns are fabricated using the electric-field and vibration-assisted AFM nanopatterning system to study the effects of different input parameters on the lithography results, which include tip bias, patterning speed, and xy in-plane vibration amplitude. To validate the effectiveness of xy in-plane vibration in the E-V AFM lithography process, multiple nanotrenches with the same speed but different tip biases are fabricated with and without xy in-plane vibration. Also, this study subsequently tested effects of x-vibration and y-vibration separately in the process. A small setpoint force ( $\sim$ 0.1 nN) and an upto-down machining direction are set for all the tests below.

Figure 2(a) shows a test result with three lines designed on the top, in which no xy-vibration is applied. The tip bias was set as 0.5, 1.2, 2 volts from the left to right lines, respectively, and the lithography speed was set as  $0.5 \,\mu\text{m/s}$  for all the lines. The bottom three lines are fabricated with 2 kHz frequency xy-vibration with 0.6 VPP amplitude. The results show that both the widths and depths increased after applying xy-vibration in the lithography

process. Notably, there is no trench fabricated when tip bias was 0.5 V for the top left-designed line, but when adding the xyvibration, the trench was fabricated with depth around 5 nm, which shows the effectiveness of mechanical vibration in the E-V AFM lithography process. Figures 2(b) and 2(c) show the height profiles of trenches fabricated without and with xy-vibration, respectively in Fig. 2(a). For the no-vibration trenches, the average depths are 0, 1.36, and 2.23 nm from left to right, with the average widths 0, 23.0, and 28.0 nm, respectively. For the xyvibration trenches, the average depths are 3.47, 5.26, and 6.83 nm, and the average widths are 34.7, 56.7, and 65.7 nm, respectively. Figure 2(d) includes a comparison of widths and depths among trenches fabricated with different input parameters. There is some debris piled up along the trench because the xy-vibration enhanced the lithography efficiency and the material removal rate. In addition, if the applied tip bias is too large in the E-AFM nanolithography process, the tip tends to be in contact with the conductive layer due to the polymer ablation and therefore creates a short circuit, which leads to the damage of the AFM tip. It is challenging yet critical to identify the appropriate tip bias that can fabricate high-resolution nanopatterns without damaging the tip. However, results show that the integration of vibration in E-V AFM process enables patterning with a very low tip bias (0.5 V), which greatly enlarges the selectable tip bias range, and therefore reduces the

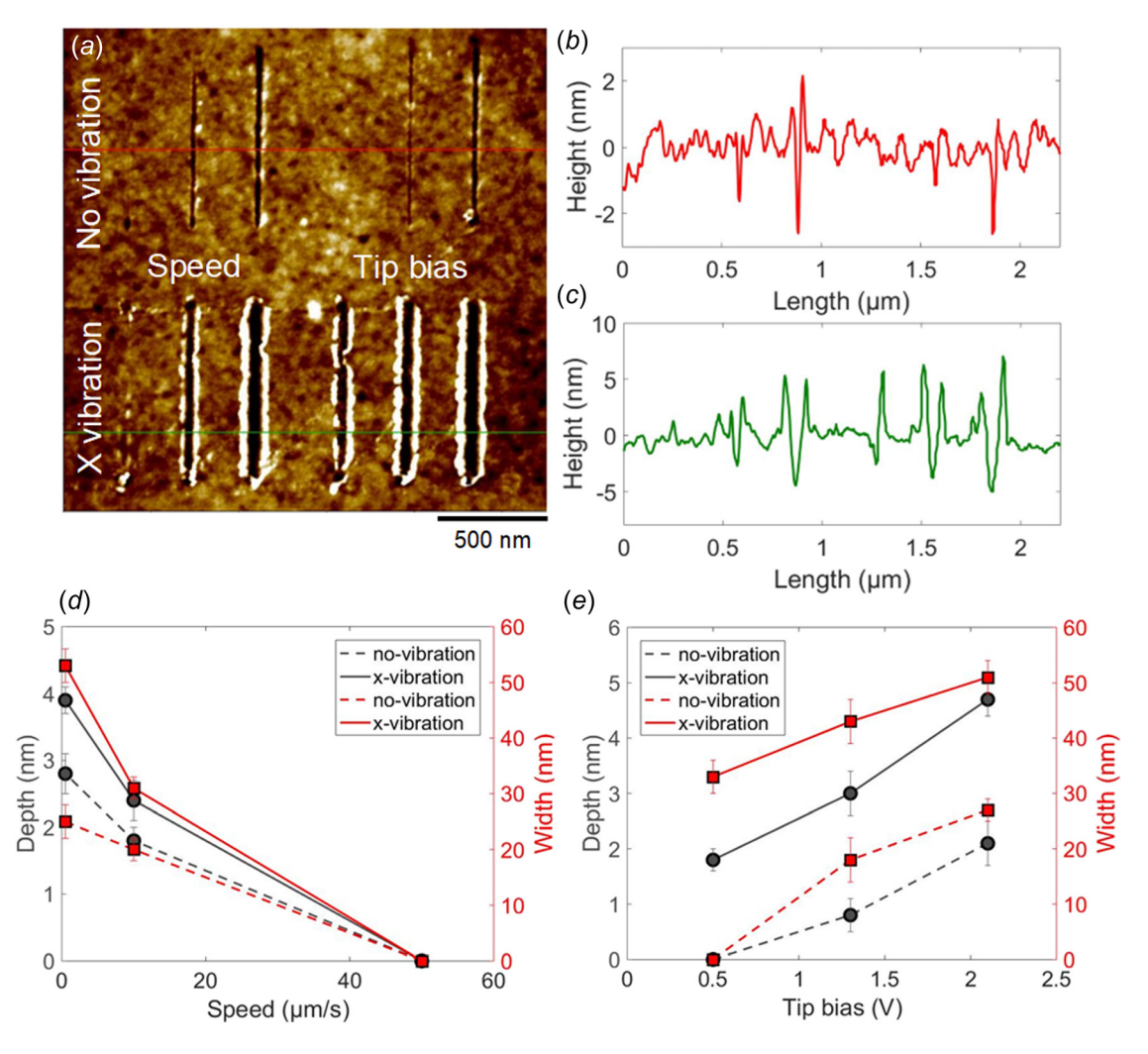


Fig. 6 E-V AFM lithography results with no-vibration and x-vibration (vibration amplitude = 0.8 VPP) comparison, with different speeds (50, 10, 0.5  $\mu$ m/s) and tip biases (0.5, 1.3, 2.1 V). (a) Topography image of nanopatterns. (b) and (c) Height profiles of nanotrenches. (d) Widths and depths of the left six trenches fabricated with and without x-vibration under different speeds. (e) Widths and depths of the right six trenches fabricated with and without x-vibration under different tip biases.

possibility of tip damage. As there are multiple ways to note trench width measurement, an illustration of the width and depth measurement methodology in added in Fig. 2(e) for clarity.

Besides the tip bias and lithography speed, the effect of the xyvibration amplitudes on the feature sizes was also investigated. Figures 3(a)-3(c) are topography images of three trenches fabricated with different xy-vibration amplitudes (0, 0.6, and 1.2 VPP) under the same tip bias (2.9 V) and the same lithography speed  $(0.5 \,\mu\text{m/s})$ . Cross-sectional profiles of the three trenches are shown in Fig. 3(d). It shows an increase of both trench width and depth as the vibration amplitude increases. Figure 3(e) shows a comparison of width and depth of trenches fabricated with different xyvibration amplitudes. The average depth of trenches fabricated with 0, 0.6, and 1.2 VPP xy-vibration applied are 0.39, 3.06, and 7.62 nm, respectively. The average width of trenches for the corresponding cases is 19.8 nm, 25.6 nm, and 55.2 nm, respectively. The results lead to the conclusion that wider and deeper patterns can be fabricated through increasing the xy-vibration amplitude under the same tip bias and speed.

In addition, the effects of x-vibration and y-vibration in the E-V AFM processes were investigated separately. As the tip feeding direction is set as vertical, these two vibration modes should have different impacts given the different vibration directions. Figure 4 shows trenches fabricated with no-vibration and x-vibration applied. The upper six lines were designed to fabricate without vibration, and the lower six lines with 0.6 VPP x-vibration. The tip bias was set as 2.1 V, and the lithography speed is 0.5  $\mu$ m/s for

all the lines. Results show an average width of about 26.5 nm, and an average depth of about 2.75 nm for the no-vibration trenches. The average width and depth for the *x*-vibration trenches were measured to be about 49.5 nm and about 3.94 nm, respectively. The comparison shows that both trench depth and width increase after applying *x*-vibration.

Another experiment was conducted by changing *x*-vibration into *y*-vibration, in which all the other input parameters were kept the same. Results are shown in Fig. 5, in which the average width is 25.2 nm, and the average depth is 2.61 nm for the no-vibration trenches. The average width and depth for the trenches fabricated under *x*-vibration are 48.7 nm and 6.07 nm, respectively. Results indicate that there is a larger increase in trench depth for the *y*-vibration applied trenches compared with the *x*-vibration applied ones, which is in consistent with the analysis of E-V AFM nanolithography mechanisms described in the previous chapter. A possible explanation is due to the differences in energy accumulation along the tip trajectory, which is constantly back and forth on the *y* direction during the lithography process.

Moreover, the effects of different input parameters (vibration status, tip bias, and nanopatterning speed) were experimentally investigated to further understand the E-V AFM process. Figure 6 shows a comparison of the topography and height profiles between trenches with no-vibration and *x*-vibration under different nanopatterning speed and tip bias. The vibration amplitude was set as 0.8 VPP. Figure 6(*a*) shows a topography image of the lithography results. For the left-hand six lines with 2.1 V tip bias,

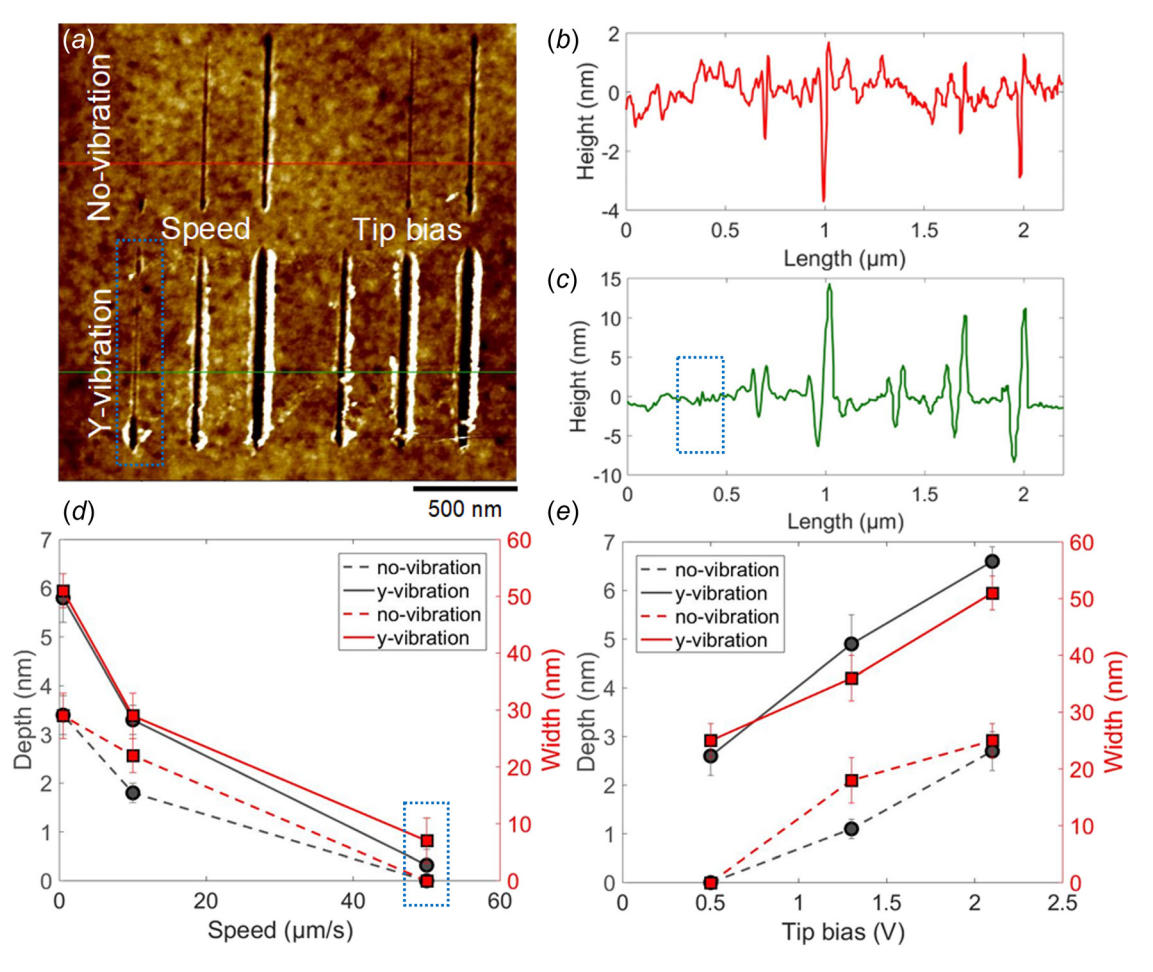


Fig. 7 E-V AFM lithography results with no-vibration and *y*-vibration (vibration amplitude = 0.8 VPP), with different speeds (50, 10,  $0.5 \mu m/s$ ) and tip biases (0.5, 1.3, 2.1 V). The dotted rectangles show feature with sub-10 nm size (close to 5 nm) under 50  $\mu$ m/s patterning speed and 2.1 V tip bias. (a) Topography image. (b) and (c) Height profiles of nanotrenches. (d) Widths and depths of the left six trenches fabricated with and without *y*-vibration under different speeds. (e) Widths and depths of the right six trenches fabricated with and without *y*-vibration under different tip biases.

their lithography speeds were set at 50, 10,  $0.5 \mu m/s$  from left to right. For the right-hand six lines with lithography speed of  $0.5 \mu \text{m/s}$ , the tip biases were set differently as 0.5, 1.3, 2.1 V. The height profiles of trenches fabricated without vibration and with xvibration are shown in Figs. 6(b) and 6(c). For the upper six lines, the average depths are 0, 1.56, 2.83, 0, 0.91, 2.37 nm from left to right, and the average widths are 0, 23.0, 25.3, 0, 19.3, 26.7 nm from left to right, respectively. For the lower six lines, the average depths are 0, 2.35, 3.99, 2.02, 2.99, 4.22 nm, and the average widths are 0, 29.0, 50.7, 35.0, 38.7, 52.5 nm from left to right, respectively. Plots that include depths and width of trenches fabricated by E-V AFM lithography with different speed and tip biases are shown in Figs. 6(d) and 6(e). Both widths and depths increase when x-vibration is applied, compared to that of the trenches without vibration. Trench depths and widths also increase as tip bias increases and when lithography speed decreases in both xvibration and no-vibration scenarios. Results show that the minimum tip bias required for patterning using E-V AFM lithography is much lower than that of the E-AFM lithography process, which leads to much less possibility of tip damage due to the tip bias value selection failure. Notably, the first line on the bottom of Fig. 6(a) has some marks that were fabricated using  $50 \,\mu\text{m/s}$  with x-vibration and 2.1 V. It demonstrates that nanopatterns can be fabricated with a much faster speed when the vibration is integrated with the electric field, which means this process greatly improves the nanopatterning efficiency and capability.

In addition, the effect of y-vibration on feature dimensions in the E-V AFM process was also investigated. Figure 7(a) includes a topography image of the lithography results. Lithography speeds of the left six lines were set as 50, 10, 0.5  $\mu$ m/s from left to right, with 2.1 V applied tip bias. The tip bias designed for the right six lines are 0.5, 1.3, 2.1 V, with lithography speed of 0.5  $\mu$ m/s. The height profiles of trenches fabricated with no-vibration and with y-vibration are shown in Figs. 7(b) and 7(c). For the upper six lines, the average depths are 0, 1.42, 3.67, 0, 1.15, 3.13 nm from left to right, respectively, and the average widths are 0, 21.7, 30.3, 0, 20.7, 26.3 nm from left to right, respectively. For the lower six lines, the average depths are 0.29, 2.86, 5.63, 2.29, 4.91, 6.04 nm, respectively, and the average widths are 7.3, 27.7, 50.7, 23.0, 38.7, 48.3 nm from left to right, respectively. Results indicate that both trench width and depth increase after adding y-vibration in the electric-field-assisted AFM lithography process. Notably, with y-vibration added in the E-AFM process, nanopatterns with sub-10 nm even approaching to sub-5 nm feature width can be fabricated, as shown in the dotted rectangles. This result marks a breakthrough in the AFM-based nanopatterning techniques and provides an alternative way to fabricate high-resolution nanopatterns with increased material removal rate, tunable feature size, and small applied mechanical force.

To confirm the advantages from the integration of electric-field and vibration, this study also included experiments with no applied tip bias but with the same force and only vibration applied as in Figs. 4 and 5, and there were no patterns fabricated. It demonstrated that the integration of both external energy forms plays a critical role in the E-V AFM nanopatterning processes, which is superior to single external energy form assisted AFM-based nanopatterning process.

### **Conclusions**

This study demonstrated a new multiple-energy-assisted AFMbased nanopatterning method through the integration of contact mode electric-field-assisted AFM lithography and in-plane xyvibration. This innovated electric-field and mechanical vibrationassisted AFM-based (E-V AFM) nanopatterning approach shows great potential for high-resolution and high-efficiency nanopatterning. As it is very challenging to identify a good tip bias range for the electric-field-assisted AFM lithography process, this new approach enables nanopatterning at lower tip bias and higher speed. The contribution of this research is as follows: First, it improves the nanopatterning capability and efficiency by enabling nanopatterning with sub-10 nm approaching to sub-5 nm feature resolution under  $50 \,\mu\text{m/s}$  patterning speed, and by increasing the feature sizes and material removal rates of single-path patterning. Second, it reduces the risk of tip damage by decreasing the minimum tip bias required for patterning and by increasing the tip bias selection range. In addition, it also reduces the debris fabricated during the nanopatterning process, as compared with the vibration-only method.

#### Acknowledgment

This work was supported in part by the National Science Foundation under Grant No. CMMI-2006127, and by the Small Scale Systems Integration and Packaging (S3IP) Center of Excellence, funded by the New York Empire State Development's Division of Science, Technology, and Innovation.

## **Funding Data**

• National Science Foundation (Award ID: CMMI-2006127; Funder ID: 10.13039/100000001).

## **Data Availability Statement**

The datasets generated and supporting the findings of this article are obtainable from the corresponding author upon reasonable request.

### References

- [1] Behzadirad, M., Mecholdt, S., Randall, J. N., Ballard, J. B., Owen, J., Rishinaramangalam, A. K., Reum, A., Gotszalk, T., Feezell, D. F., Rangelow, I. W., and Busani, T., 2021, "Advanced Scanning Probe Nanolithography Using GaN Nanowires," Nano Lett., 21(13), pp. 5493–5499.
  [2] Chang, S., Geng, Y., and Yan, Y., 2022, "Tip-Based Nanomachining on Thin
- Films: A Mini Review," Nanomanuf. Metrol., 5(1), pp. 2–22.
- [3] Gomez, J. L., and Tigli, O., 2013, "Zinc oxide Nanostructures: From Growth to Application," J. Mater. Sci, 48(2), pp. 612-624.
- [4] Wang, J., Yan, Y., Li, Z., and Geng, Y., 2021, "Towards understanding the Machining Mechanism of the Atomic Force Microscopy Tip-Based Nanomilling Process," Int. J. Mach. Tools Manuf., 162, p. 103701.
- [5] Deng, J., Jiang, L., Si, B., Zhou, H., Dong, J., and Cohen, P., 2021, "AFM-Based Nanofabrication and Quality Inspection of Three-Dimensional Nanotemplates for Soft Lithography," J. Manuf. Process, 66, pp. 565-573.
- [6] Rühe, J., 2017, "And There Was Light: Prospects for the Creation of Microand Nanostructures Through Maskless Photolithography," ACS Nano, 11(9), pp. 8537-8541.
- Wang, K., Ma, Q., Qu, C.-X., Zhou, H.-T., Cao, M., and Wang, S.-D., 2022, "Review on 3D Fabrication at Nanoscale," Autex Res. J., epub.
  [8] Harinarayana, V., and Shin, Y. C., 2021, "Two-Photon Lithography for Three-
- Dimensional Fabrication in Micro/Nanoscale Regime: A Comprehensive Review," Opt. Laser Technol., 142, p. 107180.
- [9] Lee, J. A., Lee, K.-C., Park, S. I., and Lee, S. S., 2008, "The fabrication of Carbon Nanostructures Using Electron Beam Resist Pyrolysis and Nanomachining Processes for Biosensing Applications," Nanotechnology, 19(21), p. 215302.
- [10] Pisano, F., Pisanello, M., Sileo, L., Qualtieri, A., Sabatini, B. L., De Vittorio, M., and Pisanello, F., 2018, "Focused ion Beam Nanomachining of Tapered Optical Fibers for Patterned Light Delivery," Microelectron. Eng., 195, pp. 41 - 49.
- [11] Duan, C., Wang, W., and Xie, Q., 2013, "Review article: Fabrication of Nanofluidic Devices," Biomicrofluidics, 7(2), p. 026501. [12] Garcia, R., Knoll, A. W., and Riedo, E., 2014, "Advanced scanning Probe Lith-
- ography," Nat. Nanotechnol., 9(8), pp. 577-587.
- [13] Kaestner, M., Ivanov, T., Schuh, A., Ahmad, A., Angelov, T., Krivoshapkina, Y., Budden, M., Hofer, M., Lenk, S., Zoellner, J.-P., Rangelow, I. W., Reum, A., Guliyev, E., Holz, M., and Nikolov, N., 2014, "Scanning probes in Nanostructure Fabrication," J. Vac. Sci. Technol. B, 32(6), p. 06F101.
- [14] Ryu Cho, Y. K., Rawlings, C. D., Wolf, H., Spieser, M., Bisig, S., Reidt, S., Sousa, M., Khanal, S. R., Jacobs, T. D. B., and Knoll, A. W., 2017, "Sub-10 Nanometer Feature Size in Silicon Using Thermal Scanning Probe Lith-ACS Nano, 11(12), pp. 11890-11897.
- [15] Bark, H., Kwon, S., and Lee, C., 2016, "Bias-Assisted Atomic Force Microscope Nanolithography on NbS2thin Films Grown by Chemical Vapor Deposition," J. Phys. Appl. Phys, 49(48), p. 484001.
- [16] Liu, H., Hoeppener, S., and Schubert, U. S., 2016, "Reversible Nanopatterning on Polypyrrole Films by Atomic Force Microscope Electrochemical Lithography," Adv. Funct. Mater., 26(4), pp. 614-619.

- [17] Liu, L., Shi, J., Li, M., Yu, P., Yang, T., and Li, G., 2018, "Fabrication of Sub-Micrometer-Sized MoS2 Thin-Film Transistor by Phase Mode AFM Lithography," Small, 14(49), p. 1803273.
- [18] Liu, X., Howell, S. T., Conde-Rubio, A., Boero, G., and Brugger, J., 2020, "Thermomechanical Nanocutting of 2D Materials," Adv. Mater., 32(31), p. 2001232
- [19] Lyuksyutov, S. F., Paramonov, P. B., Dolog, I., and Ralich, R. M., 2003, "Peculiarities of an Anomalous Electronic Current During Atomic Force Microscopy Assisted Nanolithography on n-Type Silicon," Nanotechnology, 14(7), pp. 716–721. [20] Zhang, L., Dong, J., and Cohen, P. H., 2013, "Material-Insensitive
- Feature Depth Control and Machining Force Reduction by Ultrasonic Vibration in AFM-Based Nanomachining," IEEE Trans. Nanotechnol., 12(5), pp.
- [21] Yao, B., Chen, C., Du, Z., Qian, Q., and Pan, L., 2022, "Surfing Scanning Probe Nanolithography at Meters per Second," Nano Lett., 22(6), pp. 2187-2193.
- [22] Chen, Y., Shu, Z., Zhang, S., Zeng, P., Liang, H., Zheng, M., and Duan, H., 2021, "Sub-10 nm Fabrication: Methods and Applications," Int. J. Extreme Manuf., 3(3), p. 032002.
- [23] Deng, J., Dong, J., and Cohen, P., 2018, "Rapid Fabrication and Characterization of SERS Substrates," Procedia Manuf., 26, pp. 580-586.
- [24] Geng, Y., Yan, Y., Wang, J., and Zhuang, Y., 2018, "Fabrication of Nanopatterns on Silicon Surface by Combining AFM-Based Scratching and RIE Methods," Nanomanuf. Metrol., 1, pp. 225-235.
- Xie, X. N., Chung, H. J., Sow, C. H., and Wee, A. T. S., 2006, "Nanoscale Materials Patterning and Engineering by Atomic Force Microscopy Nano-
- Indicriats Fauctining and Engineering by Atomic Force Microscopy Nanolithography," Mater. Sci. Eng. R: Rep., 54(1–2), pp. 1–48.
  [26] Hu, H., Kim, H. J., and Somnath, S., 2017, "Tip-Based Nanofabrication for Scalable Manufacturing," Micromachines, 8(3), p. 90.
  [27] Garcia, R., Martinez, R. V., and Martinez, J., 2006, "Nano-Chemistry and Scanning Probe Nanolithographies," Chem. Soc. Rev., 35(1), pp. 29–38.
  [28] Klehn, B., and Kunze, U., 1999, "Nanolithography With an Atomic Force Microscope by Means of Vector Scan Controlled Dynamic Planning," I. April 1997, "April 1997, "Apr
- Microscope by Means of Vector-Scan Controlled Dynamic Plowing," J. Appl. Phys., **85**(7), pp. 3897–3903.
- [29] Fang, T. H., and Chang, W. J., 2003, "Effects of AFM-Based Nanomachining Process on Aluminum Surface," J. Phys. Chem. Solids, 64(6), pp. 913–918.

- [30] Wang, J., Yan, Y., Jia, B., and Geng, Y., 2021, "Study on the Processing Outcomes of the Atomic Force Microscopy Tip-Based Nanoscratching on GaAs,' J. Manuf. Process, 70, pp. 238–247.
- [31] Deng, J., Dong, J., and Cohen, P. H., 2018, "Development and Characterization of Ultrasonic Vibration Assisted Nanomachining Process for Three-Dimensional Nanofabrication," IEEE Trans. Nanotechnol., 17(3), pp. 559–566.
- [32] Li, B., Geng, Y., and Yan, Y., 2020, "Nano/Microscale Thermal Field Distribution: Conducting Thermal Decomposition of Pyrolytic-Type Polymer by Heated AFM Probes," Nanomaterials, 10(3), p. 483.
- [33] Chang, S., Yan, Y., Li, B., and Geng, Y., 2021, "Nanoscale Manipulation of Materials Patterning Through Thermomechanical Nanolithography Using Atomic Force Microscopy," Mater. Des., 202, p. 109547
- [34] Howell, S. T., Grushina, A., Holzner, F., and Brugger, J., 2020, "Thermal Scanning Probe Lithography—a Review, Microsyst. Nanoeng, 6(1), pp. 1–24. [35] Zhou, H., Dmuchowski, C., Ke, C., and Deng, J., 2020, "External-Energy-
- Assisted Nanomachining With Low-Stiffness Atomic Force Microscopy Probes," Manuf. Lett., 23, pp. 1-4.
- [36] Ding, L., Li, Y., Chu, H., Li, C., Yang, Z., Zhou, W., and Tang, Z. K., 2007, "High Speed Atomic Force Microscope Lithography Driven by Electrostatic Interaction," Appl. Phys. Lett., 91(2), p. 023121.
- [37] Kaestner, M., and Rangelow, I. W., 2020, "Scanning probe Lithography on Calixarene Towards Single-Digit Nanometer Fabrication," Int. J. Extreme Manuf., 2(3), p. 032005.
- [38] Ryu, Y. K., and Garcia, R., 2017, "Advanced Oxidation Scanning Probe Lithography," Nanotechnology, 28(14), p. 142003.
- [39] Lyuksyutov, S. F., Paramonov, P. B., Juhl, S., and Vaia, R. A., 2003, "Amplitude-Modulated Electrostatic Nanolithography in Polymers Based on
- Atomic Force Microscopy," Appl. Phys. Lett., 83(21), pp. 4405–4407.
  [40] Zhou, H., Jiang, Y., Dmuchowski, C. M., Ke, C., and Deng, J., 2022, "Electric-Field-Assisted Contact Mode Atomic Force Microscope-Based Nanolithography With Low Stiffness Conductive Probes," ASME J. Micro Nano-Manuf., 10, p. 011001.
- Yang, Y., and Zhao, W., 2019, "Fabrication of Nanoscale to Microscale 2.5D Square Patterns on Metallic Films by the Coupling AFM Lithography," J. Manuf. Process, 46, pp. 129–138.
- [42] Zhang, L., and Dong, J., 2012, "High-Rate Tunable Ultrasonic Force Regulated Nanomachining Lithography With an Atomic Force Microscope," Nanotechnology, 23(8), p. 085303.